IOPscience iopscience.iop.org

Home Search Collections Journals About Contact us My IOPscience

Probing the electronic structure and optical response of a graphene quantum disk supported on monolayer graphene

This article has been downloaded from IOPscience. Please scroll down to see the full text article.

2012 J. Phys.: Condens. Matter 24 314213

(http://iopscience.iop.org/0953-8984/24/31/314213)

View the table of contents for this issue, or go to the journal homepage for more

Download details:
IP Address: 128.219.49.14
The article was downloaded on 24/08/2012 at 16:15

Please note that terms and conditions apply.

J. Phys.: Condens. Matter **24** (2012) 314213 (6pp) doi:10.1088/0953-8984/24/31/314213

Probing the electronic structure and optical response of a graphene quantum disk supported on monolayer graphene

Wu Zhou[1,2], **Stephen J Pennycook**[1] **and Juan-Carlos Idrobo**[1]

[1] Materials Science and Technology Division, Oak Ridge National Laboratory, Oak Ridge, TN 37831, USA
[2] Department of Physics and Astronomy, Vanderbilt University, Nashville, TN 37235, USA

E-mail: wu.zhou@vanderbilt.edu

Received 1 March 2012, in final form 30 May 2012
Published 20 July 2012
Online at stacks.iop.org/JPhysCM/24/314213

Abstract
In this paper, we show that a graphene quantum disk (GQD) can be generated on monolayer graphene via structural modification using the electron beam. The electronic structure and local optical responses of the GQD, supported on monolayer graphene, were probed with electron energy-loss spectrum imaging on an aberration-corrected scanning transmission electron microscope. We observe that for small GQD, ∼1.3 nm in diameter, the electronic structure and optical response are governed by the dominating edge states, and are distinctly different from either monolayer graphene or double-layer graphene. Highly localized plasmon modes are generated at the GQD due to the confinement from the edge of the GQD in all directions. The highly localized optical response from GQDs could find use in designing nanoscale optoelectronic and plasmonic devices based on monolayer graphene.

(Some figures may appear in colour only in the online journal)

1. Introduction

Graphene has attracted significant attention due to its exceptional properties [1, 2] and very promising applications. The successful fabrication of large sheets of graphene [3, 4] using the chemical vapor deposition (CVD) method has further stimulated the search for potential applications ranging from high frequency electronics and chemical sensors to nanophotonics and nanoplasmonics [5–13]. Among these applications, the field of graphene-based optoelectronics [12, 13] and plasmonics [8–10] is believed to be the most promising [10], which makes use of some unique optical properties of graphene. For example, plasmons in graphene [1, 2, 5, 6] can be tuned by chemical doping or electrostatic gating [7, 14, 15], and show much stronger field confinement and enhanced light–matter interactions [16]. This provides some exciting possibilities to design tunable optoelectronic [12, 13] and plasmonic devices [8, 9] at the nanometer scale based on monolayer graphene sheets.

Recent studies have shown that structural defects in monolayer graphene and graphene nanostructures can have considerably different optical properties from homogeneous graphene sheet. For example, a single point defect in graphene can act as an atomic antenna in the petahertz (10^{15} Hz) frequency range, leading to surface plasmon enhancement at the sub-nanometer scale [17]. Similarly, an enhancement of the optical response at 11 eV along the open edges of monolayer graphene, with spatial extent of ∼0.6 nm, has been observed [18], presumably arising from a new one-dimensional plasmon (or inter-band transition) mode. Theoretical calculations also suggest that when graphene is tailored into narrow ribbons [19–23] or nanodisks, the presence of edge states becomes dominant and provides an efficient way of exciting confined surface plasmons [16]. In the case of graphene nanodisks, the surface plasmons can be confined in all dimensions, and can increase the light–matter interaction to a higher phonon energy range [16]. Moreover, a recent theoretical study suggests that full optical absorption can be achieved at a specific wavelength with arrays of

 © 2012 IOP Publishing Ltd Printed in the UK & the USA

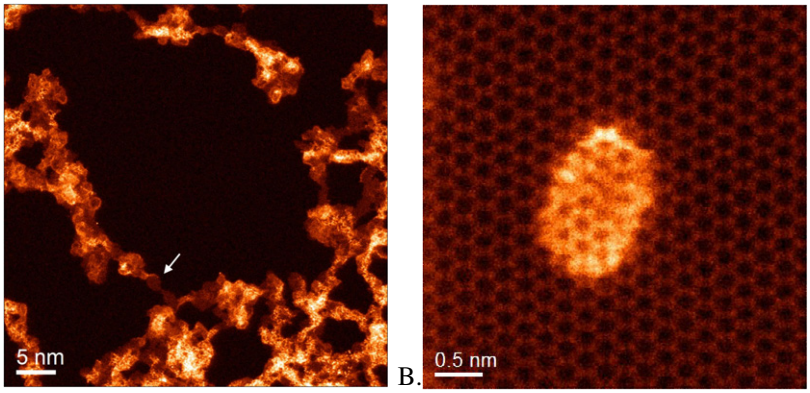

Figure 1. STEM-MAADF images of (A) patches of a second layer and multilayer on graphene and (B) a graphene quantum disk (GQD), about 1.3 nm in size, on top of monolayer graphene. The arrow highlights a narrow patch of a second graphene layer that can be transformed into a GQD via electron beam modification.

doped graphene nanodisks supported on a substrate under total internal reflection [24], which can drastically boost the efficiency of graphene-based optical devices.

In this study, we use annular dark-field (ADF) imaging and electron energy-loss (EEL) spectrum imaging on an aberration-corrected scanning transmission electron microscope (STEM) to study the atomic structure, electronic structure and local optical responses of a graphene quantum disk (GQD) supported on monolayer graphene. In particular, the density of unoccupied electronic states of the GQD was probed via the near edge fine structures in the core-loss EEL spectra. The low-loss regime of the EEL spectrum is directly related to the dielectric constant of the material, and provides rich information about the optical responses and plasmon properties of the material [25, 26]. Using low-loss EEL spectrum imaging, the local optical responses of the GQD can be measured at the nanometer scale as a function of electron-probe positions.

2. Experiments

The CVD graphene material was grown on a Cu film on a silicon wafer. The Cu film was then etched away, and the graphene layer was deposited onto a 2000 mesh copper TEM grid.

STEM-ADF imaging and EEL spectrum imaging were performed on an aberration-corrected Nion UltraSTEM [27], equipped with a cold field emission electron gun, operating at 60 kV accelerating voltage, which is below the damage threshold of the perfect graphene lattice. After aberration correction, this microscope is capable of providing an electron probe close to 1 Å diameter with a current of ∼100 pA. EEL spectra were collected using a Gatan Enfina spectrometer, with an energy resolution of 0.6 eV for 0.3 eV/channel energy dispersion. The convergence semi-angle for the incident probe was 31 mrad, with an EELS collection semi-angle of 48 mrad. ADF images were collected from ∼54 to 200 mrad half-angle range for the medium angle ADF (MAADF) or from ∼86 to 200 mrad for high angle ADF (HAADF). As limited by the dynamic range of the CCD camera in our EEL spectrometer, the highly intense zero-loss peak (ZLP) was not recorded in the spectrum image. The core-loss range of the spectrum image was filtered using the principal component analysis (PCA) [28], and reconstructed with three principal components. PCA filtering helped to reduce the noise level, but it is important to note that both the raw data and the PCA filtered data give the same fine structures in the C core-loss spectra.

3. Results and discussions

Two-dimensional structural defects are not rare in monolayer graphene materials. In particular, patches of a second layer or multilayers are commonly observed in all the CVD graphene materials we studied. These patches sometimes are quite small (see figure 1(A) for example), and their structure can be modified using the intense electron beam in STEM. This provides some opportunities to generate new types of graphene nanostructures supported on monolayer graphene through electron beam modification. One fascinating example is shown in figure 1, where a graphene quantum disk, about 1.3 nm in diameter, was generated on top of the monolayer graphene by electron beam modification of a narrow patch of a second graphene layer.

Figure 2(A) shows the ADF survey image of a GQD on monolayer graphene, which is surrounded by patches of multilayer graphene. The white square highlights the region where the EEL spectrum image was acquired. The structure of the GQD can be seen from the simultaneous HAADF image in figure 2(B), which was used to define the spatial extension of the GQD. The carbon map, extracted from the spectrum image, confirms the presence of a second carbon layer at the GQD, giving an integrated carbon signal twice as high as that from monolayer graphene.

In order to compare the electronic structure of the GQD from monolayer and double-layer graphene, we extract the core-loss spectra from the center of the GQD and from the clean area of the monolayer graphene. Carbon K-edge spectra acquired separately from monolayer and double-layer graphene were also compared. As shown in figure 3(A),

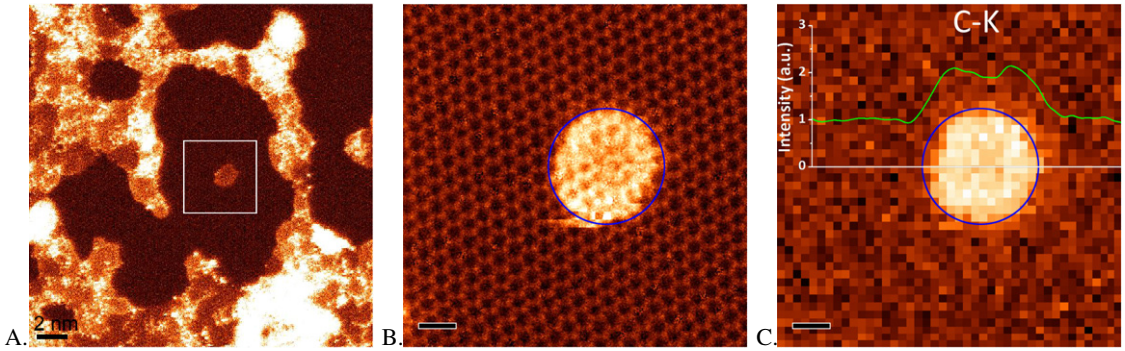

Figure 2. Core-loss spectrum images of a graphene quantum disk (GQD) on monolayer graphene. (A) HAADF survey image showing the presence of the GQD. The white square highlights the area from which the spectrum image was taken. (B) HAADF image collected simultaneously during the spectrum image. (C) C K-edge map with 40 eV integrated energy window from the onset of the C K-edge. The inset in (C) shows the normalized intensity line profile along the horizontal white line across the GQD. Scale bars in (B) and (C): 0.5 nm.

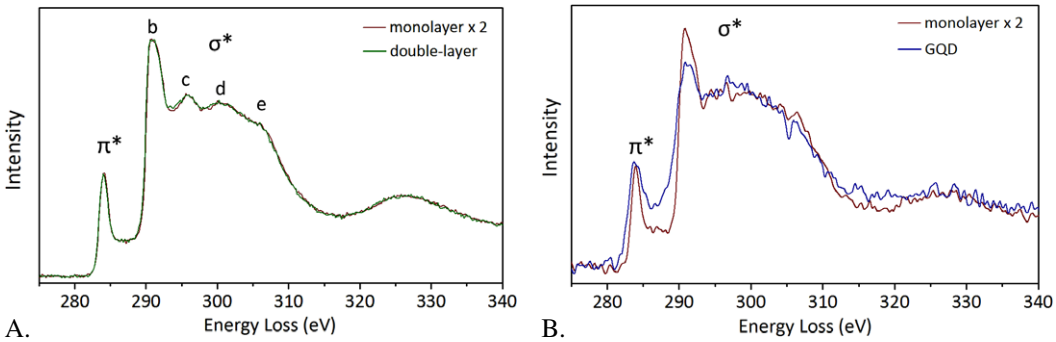

Figure 3. Comparison of the carbon K-edge core-loss spectra from (A) monolayer and double-layer graphene and (B) monolayer graphene and a GQD supported on monolayer graphene.

the carbon K-edge spectra from monolayer and double-layer graphene show exactly the same fine structures. Specifically, the spectra consist of a sharp π^* peak at the edge threshold for transitions from the carbon 1 s to π^* anti-bonding states, and four peaks, labeled b–e, for the carbon 1 s to σ^* transitions, characteristic of sp^2 hybridized carbon [29]. Since the core-loss signal is proportional to the number of atoms, the C–K intensity from double-layer graphene is approximately twice that from monolayer graphene, after normalizing with respect to the electron dose.

Even though the GQD is essentially a small patch of second layer of honeycomb carbon lattice, the core-loss spectrum from the GQD show very different features from those of continuous graphene. As shown in figure 3(B), while there is no shift for the π^* and σ^* peak positions, broadening of the peak width for both π^* and b peaks can be observed at GQD. The peak broadening also results in a red shift of the onset of the π^* and σ^* peaks from GQD to lower energies. Associated with the broadening of the b peak is a slight decrease of the peak maximum as compared to double-layer graphene. In contrast, the maximum of the π^* peak remains about twice that for monolayer graphene, giving an integrated intensity over the whole π^* peak about three times that from monolayer graphene. The increase in the integrated intensity for the π^* peak indicates the presence of more π^* anti-bonding states due to the dangling bonds of the carbon atoms on the GQD edge. The three smaller peaks, c–e, for the carbon 1 s to σ^* transitions cannot be well identified in figure 3(B) due to the relatively high noise level. However, an increase in the transition for energy-loss at ∼297 and ∼315 eV can be clearly observed at the GQD. These fine structure features were consistently observed at GQDs in all the spectrum images we obtained, and they are very similar to those obtained from the step edge of a second-layer graphene sheet on monolayer graphene due to the domination of the edge states. However, the edge electronic states seem to be more delocalized at the small GQD than on a step edge. For the 1.3 nm size GQD shown in figure 2, the C K-edge fine structure consistently reproduces that of the edge states across the whole GQD; while for a step edge on monolayer graphene, the fine structures characteristic of the edge states are confined within a ∼3 Å range, i.e. within the range of one carbon atom.

Figure 4(A) shows the low-loss EEL spectra from monolayer and double-layer graphene. The spectra were normalized with respect to the integrated intensity of the negative energy-loss part of the ZLPs (normalization with respect to the maxima of the ZLPs gives the same results). Two major absorption peaks can be observed at 5 and 15.3 eV in the low-loss spectrum from monolayer graphene, commonly referred to as the π and $\pi + \sigma$ plasmons, respectively [30]. With good energy resolution and good signal-to-noise (S/N) ratio in the experimental spectrum, one

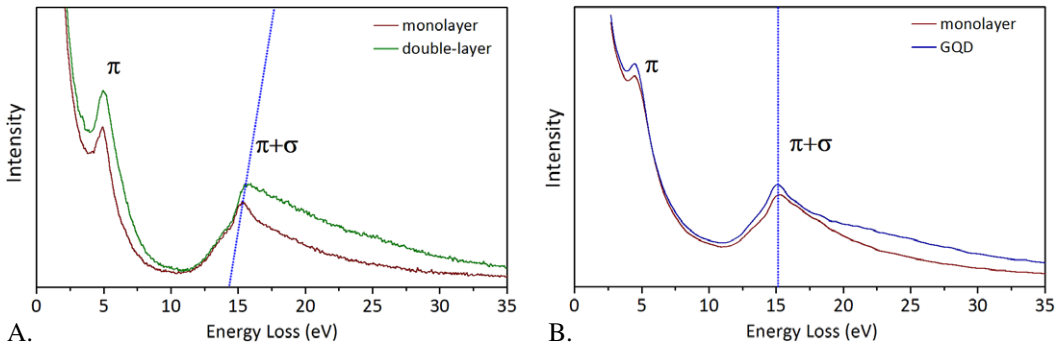

Figure 4. Comparison of the low-loss spectra from (A) monolayer and double-layer graphene and (B) monolayer graphene and a GQD supported on monolayer graphene.

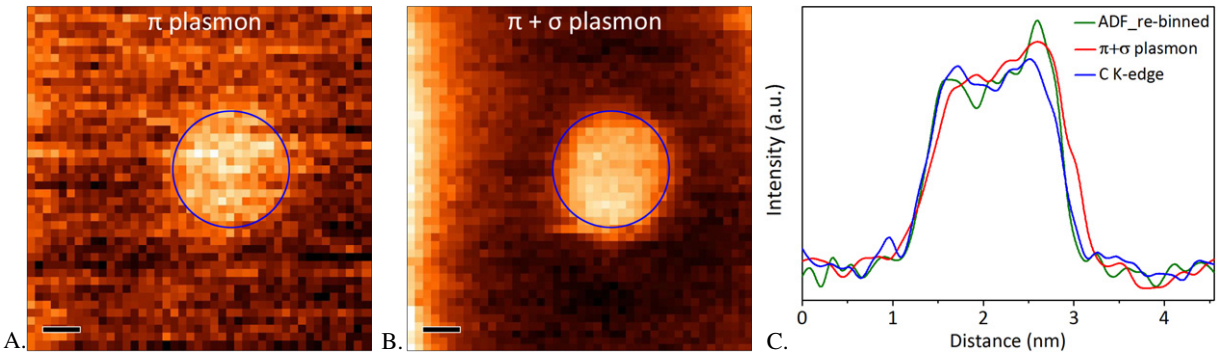

Figure 5. Plasmon maps of a graphene quantum disk on monolayer graphene: (A) plasmon map using the energy range of 4–5.5 eV; (B) $\pi + \sigma$ plasmon map using the energy range of 11.1–18 eV; (C) intensity line profiles of the simultaneous ADF image (figure 2(B), green), $\pi + \sigma$ plasmon map (red) and C K-edge map (figure 2(C), blue) taken along the vertical direction across the GQD. The blue circles highlight the spatial extent of the GQD as determined from the simultaneous ADF image in figure 2(B). Scale bars: 0.5 nm.

can also observe a weak shoulder at 13.4 eV, right before the $\pi + \sigma$ plasmons. The low-loss spectrum from double-layer graphene shows some distinct differences from monolayer graphene. Specifically, the intensity for the π plasmon for double-layer graphene was consistently increased over the whole energy range (i.e. 4–10 eV), whereas the $\pi + \sigma$ plasmon shows an asymmetric intensity increase; the intensity in the 11–15 eV range remains roughly unchanged, while the intensity in the 15–25 eV range is increased by roughly the same amount. The peak position for the π plasmon shifts by 0.05 eV towards higher energy, while the peak position for the $\pi + \sigma$ plasmon increases by 0.4 eV, shifted to 15.7 eV for double-layer graphene.

In contrast to double-layer graphene, no energy shift of the peak positions for π and $\pi + \sigma$ plasmons was observed at the GQD as shown in figure 4(B). The low-loss spectrum from the GQD shows a consistent increase in intensity over both plasmon peaks, with respect to the spectrum from monolayer graphene, but with a very different intensity distribution from the low-loss spectrum from double-layer graphene. In particular, the intensity before the maximum of the $\pi + \sigma$ plasmon at the 11–15 eV range is enhanced at the GQD, while the intensity enhancement at the 15–20 eV range, as seen for double-layer graphene, was suppressed at the GQD. Previous study has shown that an enhancement of the electronic excitations at the pre-maximum region of the $\pi + \sigma$ plasmon, most noticeable at 11 eV, can be induced by edge states [18]. The features in the low-loss spectrum of the GQD, thus suggest that the optical responses of GQD are dominated by the edge states and are different from that of a continuous double-layer graphene sheet.

As suggested by previous studies, the domination of the edge state at all dimensions can help to generate highly confined plasmons at GQD [16, 18]. The low-loss spectrum image helps to map out the spatial distribution of the π and $\pi + \sigma$ plasmons at the GQD and monolayer graphene. figures 5(A) and (B) show the two-dimensional spectroscopic maps for π and $\pi + \sigma$ plasmons using integrated energy windows of 4–5.5 eV and 11.1–18 eV, respectively. Localized enhancement can be clearly observed at the GQD in both plasmon maps with tight spatial confinement. In contrast, plasmons from monolayer or double-layer graphene typically show a long decaying tail [18] due to the delocalization of the plasmon signals. This is evident in the plasmon maps in figure 5, where the nearby continuous double-layer patches (see figure 2(A)) induce decaying background from the left side and the top-right corner of the plasmon maps. This delocalized decaying plasmon intensity is more clearly shown in figure 5(B), whereas the high noise level in the π plasmon map makes it difficult to visualize this effect in figure 5(A). The tight spatial confinement of the plasmon from GQD is further shown by the line intensity profiles

from the spectrum image. Figure 5(C) shows the intensity line profiles of the simultaneous ADF image (figure 2(B)), the C K-edge map (figure 2(C)), and the $\pi + \sigma$ plasmon map (figure 5(B)) taken along the vertical direction across the GQD. The choice of the vertical direction aims to minimize the variation in the plasmon intensity at the monolayer graphene region, induced by the nearby multilayer patches. The simultaneous ADF image was acquired with a 16 pixel × 16 pixel sub-pixel-scanning setting, and was re-binned to the same pixel size as the spectrum images for the line intensity profile. As shown in figure 5(C), the delocalization of the $\pi + \sigma$ plasmon signals from GQD is only slightly larger than that of the C K-edge signal or the ADF signal, and decreases to half of its maximum at ∼3.3Å away from the edge of the GQD. In comparison, the $\pi + \sigma$ plasmon signals at 15 eV from monolayer graphene decrease to half their maximum at ∼9 Å away from the graphene edge into vacuum [18]. This observation suggests that the optical response from the GQD is strongly influence by the edge states, and the localized plasmon response can be obtained at GQD due to the confinement from the GQD edges.

In the present case, the GQD is only 1.3 nm in diameter, and the electronic structure and optical response is dominated by the edge states. It is intuitive that the electronic and optical properties of GQD are size dependent, because when the GQD size increases to infinity, the GQD will eventually behave the same as a bilayer graphene film. A systematic study is needed in order to better understand the relationship between the local optical properties of GQDs and their size and orientation. Moreover, we find that dopant atoms, including Si, Fe, Co and Pt, tend to decorate the step edge around the second graphene layer due to the presence of unsaturated carbon atoms. It is, in principle, possible to generate metal-terminated GQDs by controlled deposition of metal atoms onto the graphene–GQD heterogeneous structure. New optical properties may emerge from this type of structure. A GQD with single metal atoms saturating the edge is analogous to a quantum corral [31], and could be used to explore the scattering and absorption of surface plasmons within the GQD.

4. Conclusions

Aberration-corrected STEM-ADF imaging and EEL spectrum imaging were applied to study the atomic structure, electronic structure and local optical responses of a graphene quantum disk supported on monolayer graphene. We show that GQDs can be created from patches of double-layer graphene supported on graphene monolayer via electron beam modification. We observe that the electronic structure and optical response of a GQD, ∼1.3 nm in size and supported on graphene monolayer, are governed by the edge states, and are distinctly different from either monolayer graphene or double-layer graphene. Highly localized plasmon modes are generated at the GQD due to the confinement from the edge of the GQD at all dimensions. By controlling the size of the GQD and the termination of the GQD edge, new optical properties may be induced at these new heterostructures. The local plasmon enhancement at the GQD and various defect sites [17, 18] also suggests that structural defects in monolayer graphene can be used as building blocks for atomic scale optoelectronic and plasmonic devices.

Acknowledgments

This research was supported by the US National Science Foundation through grant No. DMR-0938330 (WZ); Oak Ridge National Laboratory's Shared Research Equipment (ShaRE) User Facility (JCI), which is sponsored by the Office of Basic Energy Sciences, US Department of Energy; the Office of Basic Energy Sciences, Materials Sciences and Engineering Division, US Department of Energy (SJP).

References

[1] Geim A K 2009 Graphene: status and prospects *Science* **324** 1530–4
[2] Abergel D S L, Apalkov V, Berashevich J, Ziegler K and Chakraborty T 2010 Properties of graphene: a theoretical perspective *Adv. Phys.* **59** 261–482
[3] Lee S, Lee K and Zhong Z 2010 Wafer scale homogeneous bilayer graphene films by chemical vapor deposition *Nano Lett.* **10** 4702–7
[4] Lee Y *et al* 2010 Wafer-scale synthesis and transfer of graphene films *Nano Lett.* **10** 490–3
[5] Novoselov K S *et al* 2004 Electric field effect in atomically thin carbon films *Science* **306** 666–9
[6] Berger C *et al* 2004 Ultrathin epitaxial graphite: 2D electron gas properties and a route toward graphene-based nanoelectronics *J. Phys. Chem.* B **108** 19912–6
[7] Wang F *et al* 2008 Gate-variable optical transitions in graphene *Science* **320** 206–9
[8] Jablan M, Buljan H and Soljacic M 2009 Plasmonics in graphene at infrared frequencies *Phys. Rev.* B **80** 245435
[9] Mishchenko E G, Shytov A V and Silvestrov P G 2010 Guided plasmons in graphene p–n junctions *Phys. Rev. Lett.* **104** 156806
[10] Echtermeyer T J *et al* 2011 Strong plasmonic enhancement of photovoltage in graphene *Nature Commun.* **2** 458
[11] Vakil A and Engheta N 2011 Transformation optics using graphene *Science* **332** 1291–4
[12] Liu M *et al* 2011 A graphene-based broadband optical modulator *Nature* **474** 64–7
[13] Bonaccorso F, Sun Z, Hasan T and Ferrari A C 2010 Graphene photonics and optoelectronics *Nature Photon.* **4** 611–22
[14] Mak K F *et al* 2008 Measurement of the optical conductivity of graphene *Phys. Rev. Lett.* **101** 196405
[15] Chen C-F *et al* 2011 Controlling inelastic light scattering quantum pathways in graphene *Nature* **471** 617–20
[16] Koppens F H L, Chang D E and Javier Garcia de Abajo F 2011 Graphene plasmonics: a platform for strong light–matter interactions *Nano Lett.* **11** 3370–7
[17] Zhou W *et al* 2012 Atomically localized plasmon enhancement in monolayer graphene *Nature Nanotechnol.* **7** 161–5
[18] Zhou W, Pennycook S J and Idrobo J C 2012 Localization of inelastic electron scattering in the low-loss energy regime *Ultramicroscopy* at press
[19] Kosynkin D V *et al* 2009 Longitudinal unzipping of carbon nanotubes to form graphene nanoribbons *Nature* **458** 872–6
[20] Li X, Wang X, Zhang L, Lee S and Dai H 2008 Chemically derived, ultrasmooth graphene nanoribbon semiconductors *Science* **319** 1229–32

[21] Xie L *et al* 2011 Graphene nanoribbons from unzipped carbon nanotubes: atomic structures, Raman spectroscopy, and electrical properties *J. Am. Chem. Soc.* **133** 10394–7
[22] Wassmann T, Seitsonen A P, Saitta A M, Lazzeri M and Mauri F 2008 Structure, stability, edge states, and aromaticity of graphene ribbons *Phys. Rev. Lett.* **101** 096402
[23] Wang X *et al* 2011 Graphene nanoribbons with smooth edges behave as quantum wires *Nature Nanotechnol.* **6** 563–7
[24] Thongrattanasiri S, Koppens F H L and Javier Garcia de Abajo F 2012 Complete optical absorption in periodically patterned graphene *Phys. Rev. Lett.* **108** 047401
[25] Erni R and Browning N D 2005 Valence electron energy-loss spectroscopy in monochromated scanning transmission electron microscopy *Ultramicroscopy* **104** 176–92
[26] Browning N D, Arslan I, Erni R and Reed B W 2011 Low-Loss EELS in the STEM *Scanning Transmission Electron Microscopy: Imaging and Analysis* ed S J Pennycook and P D Nellist (New York: Springer)
[27] Krivanek O L *et al* 2008 An electron microscope for the aberration-corrected era *Ultramicroscopy* **108** 179–95
[28] Watanabe M, Okunishi E and Ishizuka K 2009 Analysis of spectrum-imaging datasets in atomic-resolution electron microscopy *Microsc. Anal.* **23** 5–7
[29] Rosenberg R A, Love P J and Rehn V 1986 Polarization-dependent C(K) near-edge x-ray-absorption fine structure of graphite *Phys. Rev.* B **33** 4034–7
[30] Gass M H *et al* 2008 Free-standing graphene at atomic resolution *Nature Nanotechnol.* **3** 676–81
[31] Crommie M F, Lutz C P and Eigler D M 1993 Confinement of electrons to quantum corrals on a metal surface *Science* **262** 218–20